

1 The suspended small-particles layer in the oxygen-poor Black Sea: a 2 proxy for delineating the effective N₂-yielding section

3 Rafael Rasse¹, Hervé Claustre¹, and Antoine Poteau¹

4 ¹Sorbonne Université and CNRS, Laboratoire d'Océanographie de Villefranche (LOV) UMR7093, Institut de la Mer de
5 Villefranche (IMEV), 06230, Villefranche-sur-Mer, France.

6

7 *Correspondence to:* rafael.rasse@obs-vlfr.fr; rjrasse@gmail.com

8 **Abstract.** The shallower oxygen-poor water masses of the ocean confine a majority of the microbial communities that can
9 produce up to 90% of oceanic N₂. This effective N₂-yielding section encloses a suspended small-particle layer, inferred from
10 particle backscattering (b_{bp}) measurements. It is thus hypothesized that this layer (hereafter, the b_{bp} -layer) is linked to microbial
11 communities involved in N₂-yielding such as nitrate-reducing SAR11 as well as sulphur-oxidizing, anammox and denitrifying
12 bacteria — a hypothesis yet to be evaluated. Here, data collected by three BGC-Argo floats deployed in the Black Sea are used
13 to investigate the origin of this b_{bp} -layer. To this end, we evaluate how the key drivers of N₂-yielding bacteria dynamics impact
14 on the vertical distribution of b_{bp} and the thickness of the b_{bp} -layer. In conjunction with published data on N₂ excess, our results
15 suggest that the b_{bp} -layer is at least partially composed of the bacteria driving N₂ yielding for three main reasons: (1) strong
16 correlations are recorded between b_{bp} and nitrate; (2) the top location of the b_{bp} -layer is driven by the ventilation of oxygen-
17 rich subsurface waters, while its thickness is modulated by the amount of nitrate available to produce N₂; (3) the maxima of
18 both b_{bp} and N₂ excess coincide at the same isopycnals where bacteria involved in N₂ yielding coexist. We thus advance that
19 b_{bp} and O₂ can be exploited as a combined proxy to delineate the N₂-yielding section of the Black Sea. This proxy can
20 potentially contribute to refining delineation of the effective N₂-yielding section of oxygen-deficient zones via data from the
21 growing BGC-Argo float network.

22 1 Introduction

23 Oxygen-poor water masses (O₂ < 3 μ M) host the microbial communities that produce between 20-40% of oceanic N₂ mainly
24 via heterotrophic denitrification and anaerobic oxidation of ammonium (Gruber and Sarmiento, 1997; Devries et al. 2013;
25 Ward 2013). The shallower oxygen-poor water masses (~50-200 m) are the most effective N₂-producing section because this
26 is where the microbial communities that condition the process mainly develop and generate up to 90% of the N₂ (Ward et al.,
27 2009; Dalsgaard et al., 2012; Babin et al., 2014). These microbial communities include nitrate-reducing SAR11, and anammox,
28 denitrifying, and sulphur-oxidizing bacteria (e.g. Canfield et al., 2010; Ulloa et al., 2012; Ward 2013; Tsementzi et al., 2016;
29 Callbeck et al., 2018). It is thus important to unravel the biogeochemical parameters that trigger the accumulation of such
30 bacteria in the ocean's oxygen-poor water masses. This information is crucial for understanding and quantifying how bacterial
31 biomass and related N₂ yielding bacteria can respond to the ongoing expansion of oceanic regions with low oxygen (Keeling
32 and Garcia, 2002; Stramma et al., 2008; Helm et al., 2011; Schmidtko et al., 2017). Ultimately, greater accuracy in this domain
33 can contribute to improving mechanistic predictions on how such expansion affects the oceans' role in driving the Earth's
34 climate by sequestering atmospheric carbon dioxide (e.g. Oschlies et al., 2018).

35 In oxygen-poor water masses, the biogeochemical factors that can affect the abundance of denitrifying and anammox bacteria
36 are the levels of O₂, organic matter (OM), nitrate (NO₃⁻), ammonium (NH₄⁺), and hydrogen sulfide (H₂S) (Murray et al., 1995;

37 Ward et al., 2008; Dalsgaard et al., 2014; Bristow et al., 2016). Therefore, to elucidate what triggers the confinement of such
38 bacteria, we need to investigate how the above biogeochemical factors drive their vertical distribution, with high temporal and
39 vertical resolution. To this end, we should develop multidisciplinary approaches that allow us to permanently monitor the full
40 range of biogeochemical variables of interest in oxygen-poor water masses.

41 Optical proxies of tiny particles can be applied as an alternative approach to assess the vertical distribution of N₂-yielding
42 microbial communities in oxygen-poor water masses (Naqvi et al., 1993). For instance, nitrate-reducing SAR11, and
43 anammox, denitrifying, and sulphur-oxidizing bacteria are found as free-living bacteria (0.2-2 μ m), and can be associated with
44 small suspended (> 2-30 μ m), and large sinking (> 30 μ m) particles (Fuchsman et al., 2011, 2012a, 2017; Ganesh et al., 2014,
45 2015). Therefore, particle backscattering (b_{bp}), a proxy for particles in the ~0.2-20 μ m size range (Stramski et al., 1999, 2004;
46 Organelli et al., 2018), can serve to detect the presence of these free-living bacteria and those associated with small suspended
47 particles.

48 Time series of b_{bp} acquired by biogeochemical Argo (BGC-Argo) floats highlight the presence of a permanent layer of
49 suspended small particles in shallower oxygen-poor water masses (b_{bp} -layer) (Whitmire et al., 2009; Wojtasiewicz et al., 2018).
50 It has been hypothesized that this b_{bp} -layer is linked to N₂-yielding microbial communities such as nitrate-reducing SAR11,
51 and denitrifying, anammox, and sulphur-oxidizing bacteria. However, this hypothesis has not yet been clearly demonstrated.
52 To address this, the first step is to evaluate: (1) potential correlations between the biogeochemical factors that control the
53 presence of the b_{bp} -layer and such arrays of bacteria (O₂, NO₃⁻, OM, H₂S; Murray et al., 1995; Ward et al., 2008; Fuchsman et
54 al., 2011; Ulloa et al., 2012; Dalsgaard et al., 2014; Bristow et al., 2016), and (2) the possible relationship between the b_{bp} -
55 layer and N₂ produced by microbial communities.

56 This first step is thus essential for identifying the origin of the b_{bp} -layer and, ultimately, determining if BGC-Argo observations
57 of b_{bp} can be implemented to delineate the oxygen-poor water masses where such bacteria are confined. The Black Sea appears
58 as a suitable area for probing into the origin of the b_{bp} -layer in low-oxygen waters in this way. It is indeed a semi-enclosed
59 basin with permanently low O₂ levels where N₂ production and related nitrate-reducing SAR11, and denitrifying and anammox
60 bacteria are mainly confined within a well-defined oxygen-poor zone (Kuypers et al., 2003; Konovalov et al., 2005; Kirkpatrick
61 et al., 2012). In addition, a permanent b_{bp} -layer is a typical characteristic of this region, which is linked to such microbial
62 communities and inorganic particles (Stanev et al., 2017, 2018, see details in section 2.0).

63 The goal of our study is therefore to investigate the origin of the b_{bp} -layer in the oxygen-poor waters of the Black Sea using
64 data collected by BGC-Argo floats. More specifically, we aim to evaluate, within the oxygen-poor zone, how: (1) two of the
65 main factors (O₂ and NO₃⁻) that drive the dynamics of denitrifying and anammox bacteria, impact on the location and thickness
66 of the b_{bp} -layer, (2) NO₃⁻ controls the vertical distribution of b_{bp} within this layer, (3) temperature drives the formation of the
67 b_{bp} -layer and consumption rates of NO₃⁻, and (4) particle content inferred from b_{bp} and N₂ produced by microbial communities
68 can be at least qualitatively correlated. Ultimately, our findings allow us to infer that b_{bp} can potentially be used to detect the
69 presence of the microbial communities that drive N₂ production in oxygen-poor water masses – *including nitrate-reducing*
70 *SAR11, and sulphur- oxidizing, denitrifying and anammox bacteria.*

71 **2.0. Background-nature of the small particles contributing to the b_{bp} -layer and their links with N₂ yielding**

72 The oxygen-poor water masses of the Black Sea are characterized by a permanent layer of suspended small particles constituted
73 of organic and inorganic particles (Murray et al., 1995; Kuypers et al., 2003; Konovalov et al., 2005; Kirkpatrick et al., 2012).
74 In the oxygen-poor (O₂< 3 μ M) section with detectable NO₃⁻, and undetectable H₂S levels, organic particles are mainly linked

75 to microbial communities involved in the production of N₂, and these include nitrate-reducing SAR11, and anammox,
76 denitrifying, and sulphur-oxidizing bacteria (Kuypers et al., 2003; Lam et al., 2007; Yakushev et al., 2007; Fuchsman et al.,
77 2011; Kirkpatrick et al., 2012). The first group listed, SAR11, provides NO₂⁻ for N₂ yielding, and makes the largest contribution
78 (20-60%) to N₂ yielding bacteria biomass (Fuchsman et al., 2011, 2017; Tsementzi et al., 2016). Meanwhile, the second and
79 third groups of bacteria make a smaller contribution to microbial biomass (~10%; e.g. Fuchsman et al., 2011, 2017) but
80 dominate N₂ yielding via anammox (NO₂⁻ + NH₄⁺ → N₂ + 2H₂O) and heterotrophic denitrification (NO₃⁻ → NO₂⁻ → N₂O → N₂)
81 (Murray et al., 2005; Kirkpatrick et al., 2012; Devries et al., 2013; Ward, 2013). The last group can potentially produce N₂ via
82 autotrophic denitrification (e.g. 3H₂S + 4NO₃⁻ + 6OH⁻ → 3SO₄²⁻ + 2N₂ + 6H₂O; Sorokin, 2002; Konovalov et al., 2003;
83 Yakushev et al., 2007). Finally, *Epsilonproteobacteria* are the major chemoautotrophic bacteria that form organic particles in
84 the sulfidic zone (e.g. oxygen-poor section with detectable sulphide levels (> 0.3 μM) but undetectable NO₃⁻; Coban-Yildiz et
85 al., 2006; Yilmaz et al., 2006; Grote et al., 2008; Canfield and Thamdrup, 2009; Glaubitz et al., 2010; Ediger et al., 2019).
86 However, they can also be involved in the production of N₂ and linked formation of organic particles in the oxygen-poor
87 section with detectable levels of sulphide and NO₃⁻ (see Figure 1, e.g. *Epsilonproteobacteria* *Sulfurimonas* acting as an
88 autotrophic denitrifier; Glaubitz et al., 2010; Fuchsman et al., 2012b; Kirkpatrick et al., 2018).

89 The inorganic component is mainly due to sinking particles of manganese oxides (Mn, III, IV) that are formed due to the
90 oxidation of dissolved Mn (II, III) pumped from the sulfidic zone (e.g. 2Mn²⁺(l) + O₂ + 2H₂O → 2MnO₂(s) + 4H⁺; Konovalov
91 et al., 2003; Clement et al., 2009; Dellwig et al., 2010). Ultimately, sinking particles of manganese oxides are dissolved back
92 to Mn (II, III), mainly via chemosynthetic bacteria that drive sulphur reduction (e.g. HS⁻ + MnO₂(s) + 3H⁺ → S⁰ + Mn²⁺(l) +
93 2H₂O; Jorgensen et al., 1991; Konovalov et al., 2003; Johnson, 2006; Yakushev et al., 2007; Fuschman et al., 2011; Stanev et
94 al., 2018). Overall, these arrays of bacteria mediate the reactions described above by using electron acceptors according to the
95 theoretical “electron tower” (e.g., O₂ → NO₃⁻ → Mn(IV) → Fe(III) → SO₄²⁻; Stumm and Morgan, 1970; Murray et al., 1995;
96 Canfield and Thamdrup, 2009). Therefore, the vertical distributions of NO₃⁻, N₂ excess, and content of small particles are
97 driven by the reactions that occur in the chemical zones of oxygen-poor water masses (e.g. nitrogenous and manganous zones,
98 which correspond to the sections where NO₃⁻ and Mn(IV), respectively, are predominantly used as electron acceptors; Murray
99 et al., 1995; Konovalov et al., 2003; Yakushev et al., 2007; Canfield and Thamdrup, 2009; see also sections 4.2 and 4.3).

100 3 Methods

101 3.1 Bio-optical and physicochemical data measured by BGC-Argo floats

102 We used data collected by three BGC-Argo floats that profiled at a temporal resolution of 5-10 days in the first 1000 m depth
103 of the Black Sea from December 2013 to July 2019 (Figure 1). These floats — allocated the World Meteorological
104 Organization (WMO) numbers 6900807, 6901866, and 7900591 — collected 239, 301, and 518 vertical profiles, respectively.
105 BGC-Argo float 6901866 was equipped with four sensors: (1) a SBE-41 CP conductivity-T-depth sensor (Sea-Bird Scientific),
106 (2) an Aanderaa 4330 optode (serial number:1411; O₂ range: 0-1000 μM, with an accuracy of 1.5%), (3) a WETLabs ECO
107 Triplet Puck, and (4) a Satlantic Submersible Ultraviolet Nitrate Analyzer (SUNA). These sensors measured upward profiles
108 of: (1) temperature (T), conductivity, and depth, (2) dissolved oxygen (O₂), (3) chlorophyll fluorescence, total optical
109 backscattering (particles + pure seawater) at 700 nm and fluorescence by Colored Dissolved Organic Matter, and (4) nitrate
110 (NO₃⁻; detection limit of ~0.5 μM with T/salinity correction processing) and bisulfide (HS⁻, detection limit of ~0.5 μM; Stanev
111 et al., 2018). Floats 6900807 and 7900591 were equipped with only the first three sensors.

112 Raw data of fluorescence and total backscattering were converted into Chlorophyll concentration (*chl*) and particle
113 backscattering (b_{bp}) following standard protocols, respectively (Schmechtig et al., 2014, 2015). Spike signals in vertical
114 profiles of *chl* and b_{bp} and due to particle aggregates were removed by using a median filter with a window size of three data
115 points (Briggs et al., 2011). NO_3^- , HS^- and O_2 data were processed following BGC-Argo protocols (Bittig and Körtzinger,
116 2015; Johnson et al., 2018; Thierry et al., 2018). Sampling regions covered by the three floats encompassed most of the Black
117 Sea area (Figure 1, and Appendix A). However, we only used data collected during periods without a clear injection of small
118 particles derived from the productive layer and Bosphorus plume (e.g. advection of water masses, Stanev et al., 2017). This
119 restriction allowed us to focus on the *in-situ* 1D processes driving local formation of the b_{bp} -layer, with minimal interference
120 from any possible external sources of small particles.

121 We only describe the time series of data collected by float 6901866 because this was the only float carrying a $\text{NO}_3^-/\text{HS}^-$ sensor.
122 Data acquired by floats 6900807 and 7900591 are described in Appendix A, and nevertheless used as complementary data to
123 those of float 6901866 to corroborate: (1) qualitative correlations between O_2 levels and the location of the b_{bp} -layer, and (2)
124 consistency in the location of the b_{bp} maximum within the b_{bp} -layer.

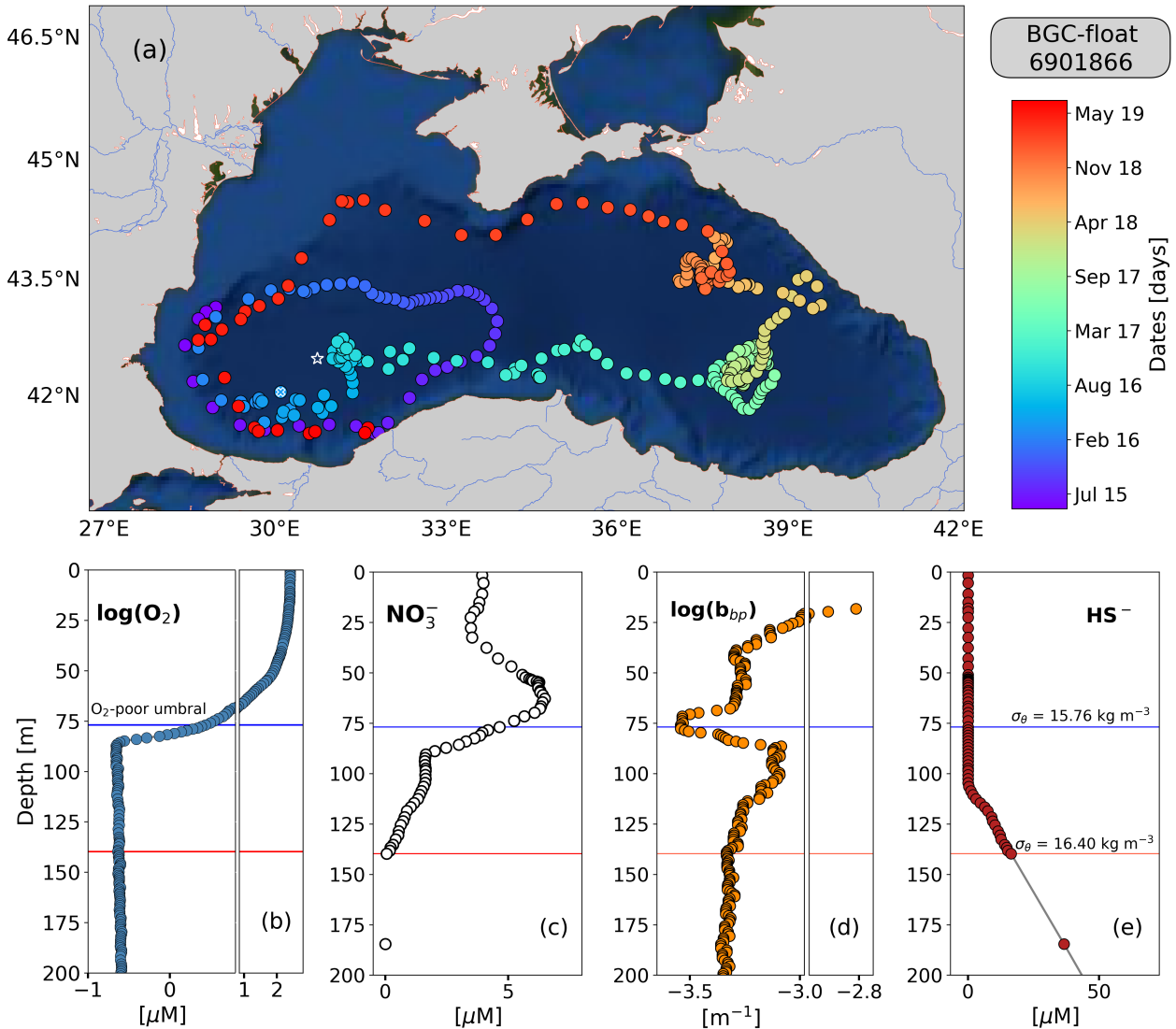
125 **3.2 Defining the oxygen-poor zone, mixed layer depth, and productive layer**

126 We used O_2 and NO_3^- to respectively define the top and bottom isopycnals of the oxygen-poor zone where denitrifying and
127 anammox bacteria are expected to be found. To set the top isopycnal, we applied an O_2 threshold of $\sim 3 \mu\text{M}$ because denitrifying
128 and anammox bacteria seem to tolerate O_2 concentrations beneath this threshold (Jensen et al., 2008; Dalsgaard et al., 2014;
129 Babbin et al., 2014). The bottom isopycnal was defined as the deepest isopycnal at which NO_3^- was detected by the SUNA
130 sensor ($0.23 \pm 0.32 \mu\text{M}$). NO_3^- was used to set this isopycnal because heterotrophic denitrification and subsequent reactions
131 cannot occur without NO_3^- (Lam et al., 2009; Bristow et al., 2017). HS^- was not used to delimit the bottom of this zone because
132 the maximum concentration of HS^- that denitrifying and anammox bacteria tolerate is not well established (Murray et al., 1995;
133 Kirkpatrick et al., 2012; see also section 4.1).

134 Mixed layer depth (MLD) was computed as the depth at which density differed from 0.03 kg m^{-3} with respect to the density
135 recorded at 1m depth (de Boyer Montégut et al., 2004). We used *chl* to define the productive layer where living phytoplankton
136 were present and producing particulate organic carbon. The base of this layer was set as the depth at which *chl* decreased
137 below 0.25 mg m^{-3} . This depth was used only as a reference to highlight the periods when surface-derived small particles were
138 clearly injected into the oxygen-poor zone.

139 **3.3 Complementary cruise data on N_2 excess and NO_3^-**

140 Published data on $\text{N}_2:\text{Ar}$ ratios and NO_3^- collected at the southwest of the Black Sea in March 2005 (Fuchsman et al., 2008,
141 2019) were exploited to complement discussion of our results. N_2 produced by anaerobic microbial communities (N_2 excess,
142 μM) was estimated from $\text{N}_2:\text{Ar}$ ratios and argon concentrations at atmospheric saturation (Hamme and Emerson, 2004). N_2
143 excess data were used to: (1) describe the oxygen-poor zone where N_2 is expected to be predominantly produced, and (2)
144 highlight qualitative correlations between N_2 excess, the location of the b_{bp} -layer, and vertical distribution of small particles
145 within the b_{bp} -layer.



146

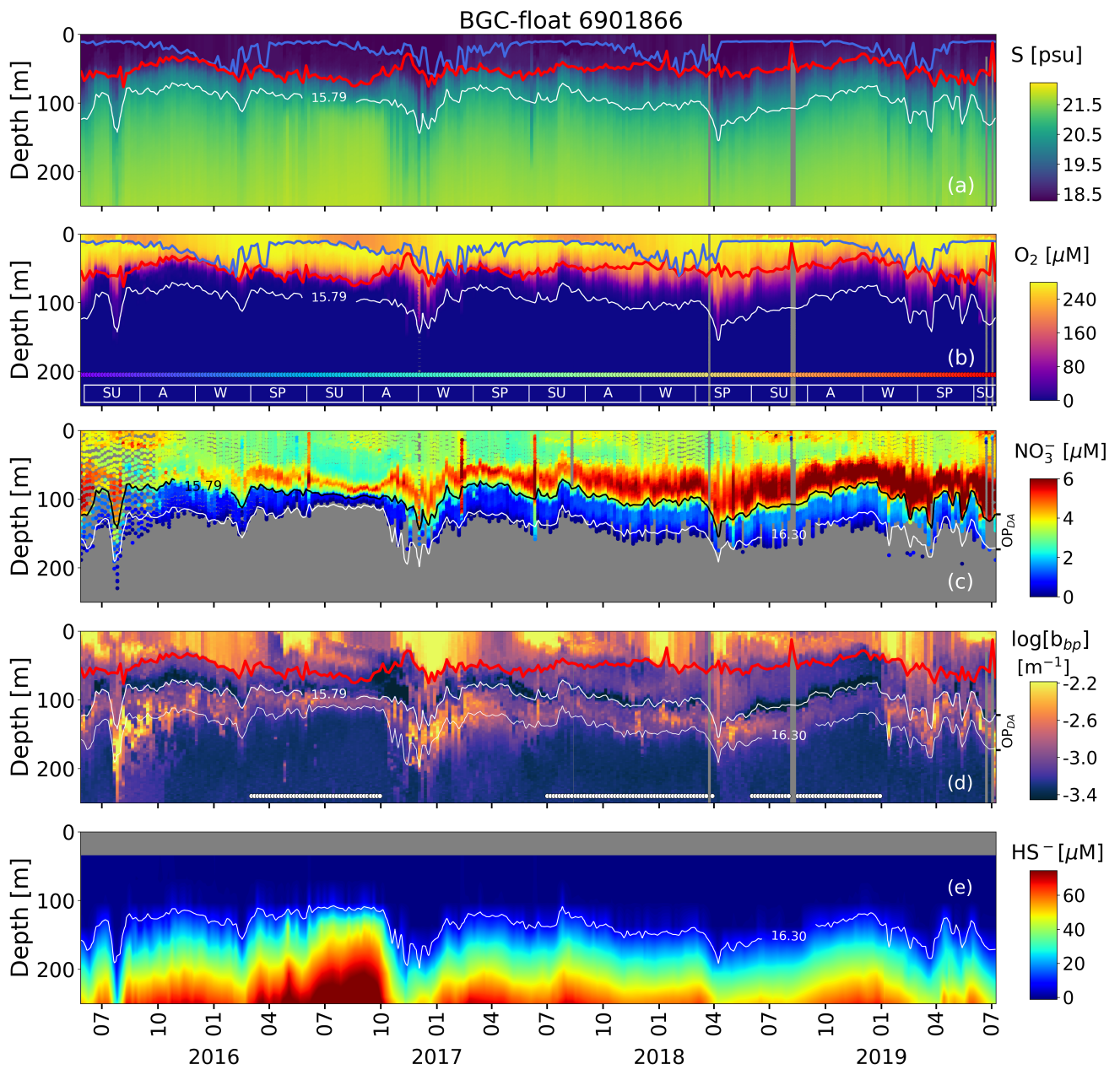
147 **Figure 1: (a) Sampling locations of float 6901866 between May 2015 and July 2019. Colored circles indicate the date**
 148 **(color bar) for a given profile. The white star in (a) marks the sampling site of the cruise (March 2005). The white x in**
 149 **(a) highlights the float location on 6th April 2016. Float profiles of (b) log(O₂), (c) NO₃⁻, (d) log(b_{bp}), and (e) HS⁻ collected**
 150 **on 24th November 2018.**

151 **4 Results and discussion**

152 **4.1 Description of the oxygen-poor zone**

153 The top and bottom of the oxygen-poor zone are located around the isopycnals (mean \pm standard deviation) $15.79 \pm 0.23 \text{ kg m}^{-3}$
 154 and $16.30 \pm 0.09 \text{ kg m}^{-3}$, respectively. The two isopycnals therefore delimit the oxygen-poor water masses where nitrate-
 155 reducing SAR11, and denitrifying, anammox, and sulphur-oxidizing bacteria are expected to be found (zone hereafter called
 156 the OP_{D-A} , Figure 2; Kuypers et al., 2003; Lam et al., 2007; Yakushev et al., 2007; Fuschman et al., 2011; Kirkpatrick et al.,
 157 2012). The top location of the OP_{D-A} shows large spatial-temporal variability ranging between 80-180 m (or σ_θ between 15.5-
 158 15.9 kg m^{-3} , Figure 2). Similarly, the OP_{D-A} thickness varies between 30-80 m, which corresponds to a σ_θ separation of ~ 0.50
 159 kg m^{-3} . The bottom of the OP_{D-A} is slightly sulfidic ($\text{HS}^- = 11.4 \pm 3.53 \mu\text{M}$, $n = 86$) and deeper than suggested (e.g. $\sigma_\theta = 16.20$

160 kg m⁻³, and H₂S \leq 10 nM, Murray et al., 1995). However, our results coincide with the slightly sulfidic conditions of the deepest
 161 isopycnal at which anammox bacteria can be still recorded ($\sigma_0 = 16.30$ kg m⁻³, and H₂S \geq 10 μ M; Kirkpatrick et al., 2012).



162
 163 **Figure 2:** Time series of: (a) Salinity (S), (b) O₂, (c) NO₃⁻, (d) log(b_{bp}), and (e) HS⁻. The blue lines in (a) and (b) indicate
 164 the mixed layer depth. The red lines in (a), (b) and (d) show the base of the productive region. The isopycnals 15.79 kg
 165 m⁻³ and 16.30 kg m⁻³ describe the top and bottom of the oxygen-poor zone (OP_{D-A}), respectively. SU, A, W, and SP stand
 166 for summer, autumn, winter, and spring, respectively. The colored horizontal line in (b) indicates the sampling site for
 167 a given date (Figure 1). The horizontal white lines in (d) are the profiles used to: (1) delimit the OP_{D-A}, and (2) compute
 168 correlations between b_{bp} , NO₃⁻, and T within the OP_{D-A}.

169 **4.2 NO₃⁻, O₂, and MnO₂ as key drivers of the thickness and location of the suspended small-particle layer**

170 The permanent b_{bp} -layer is always confined within the two isopycnals that delimit the OP_{D-A} (Figure 2). It follows that the
 171 thickness and top location of this layer demonstrate the same spatial and temporal variability as the one described for the OP_D.

172 A (Figure 2 and Appendix A). This correlation indicates that variations in the thickness and top location of the b_{bp} -layer are
173 partially driven, respectively, by: (1) the amount of NO_3^- available to produce N_2 inside the $OP_{D,A}$ via the set of bacteria
174 communities involved, and (2) downward ventilation of oxygen-rich subsurface waters (Figure 2 and Appendix A).

175 NO_3^- and O_2 are two of the key factors that modulate the presence of: (1) denitrifying and anammox bacteria working in
176 conjunction with nitrate-reducing SAR11 (Fuschman et al., 2011; Ulloa et al., 2012; Tsementzezi et al., 2016; Bristow et al.,
177 2017), and probably with chemoautotrophic ammonia-oxidizing bacteria (in this case, only with anammox, e.g. γ AOB; Ward
178 and Kilpatrick, 1991; Lam et al., 2007), and (2) sulphur-oxidizing bacteria (e.g. SUP05 and potentially *Epsilonproteobacteria*
179 *Sulfurimonas*; Canfield et al., 2010; Glaubitz et al., 2010; Fuschman et al., 2011, 2012b; Ulloa et al., 2012; Kirkpatrick et al.,
180 2018). Therefore, the results described above highlight that at least a fraction of the b_{bp} -layer should be due to this array of
181 bacteria. This notion is supported by three main observations. Firstly, the top location of the b_{bp} -layer is driven by the intrusion
182 of subsurface water masses ($S \leq 20.36 \pm 0.18 \text{ psu}$) with O_2 concentrations above the levels tolerated by denitrifying and
183 anammox bacteria ($\text{O}_2 \geq 3 \mu\text{M}$, Jensen et al., 2008; Babbin et al., 2014; Figure 2). As a result, in regions where O_2 is ventilated
184 to deeper water masses, the top location of the b_{bp} -layer is also deeper. The contrary is observed when O_2 ventilation is
185 shallower (Figure 2 and Appendix A). Secondly, nitrate-reducing SAR11, and denitrifying, anammox, and sulphur-oxidizing
186 bacteria reside between the isopycnals 15.60-16.30 kg m^{-3} (Fuchsman et al., 2011; 2012a; Kirkpatrick et al., 2012), while the
187 b_{bp} -layer is formed between isopycnals ~ 15.79 -16.30 kg m^{-3} . We can thus infer coexistence of such bacteria between the
188 coincident isopycnals where the b_{bp} -layer is generated. Thirdly, NO_3^- declines from around isopycnal 15.79 kg m^{-3} to the
189 isopycnal 16.30 kg m^{-3} due to the expected N_2 production via the microbial communities involved (Figures 2-3, and Kirkpatrick
190 et al., 2012).

191 The ventilation of subsurface O_2 is also key in driving the depth at which MnO_2 is formed ($\text{O}_2 \leq 3-5 \mu\text{M}$; Clement et al., 2009),
192 and can thus contribute to setting the characteristics of the b_{bp} -layer via its subsequent accumulation and dissolution
193 (Konovalov et al., 2003; Clement et al., 2009; Dellwig et al., 2010). Thus, in regions where subsurface O_2 (e.g. $\text{O}_2 \geq 3-5 \mu\text{M}$,
194 and $S \leq 20.36 \pm 0.18 \text{ psu}$) is ventilated to deeper water masses, both the formation of MnO_2 and top location of the b_{bp} -layer
195 can be expected to be deeper, and vice versa (Figure 2). Finally, the dissolution of MnO_2 should also influence the thickness
196 of the b_{bp} -layer because it occurs just beneath the maxima of the optical particles inside this layer (Konovalov et al., 2006; see
197 the explanation in section 4.3).

198 Overall, the qualitative evidence presented above points out that particles of MnO_2 as well as nitrate-reducing SAR11, and
199 denitrifying, anammox, and sulphur-oxidizing bacteria, appear to define the characteristics of the b_{bp} -layer (Johnson, 2006;
200 Konovalov et al., 2003; Fuchsman et al., 2011, 2012b; Stanev et al., 2018). This observation leads us to argue, in the next
201 section, that the b_{bp} -layer is partially composed of the main group of microbial communities involved in N_2 yielding, as well
202 as of MnO_2 .

203 **4.3 Role of the removal rate of NO_3^- , MnO_2 , and temperature in the vertical distribution of small particles**

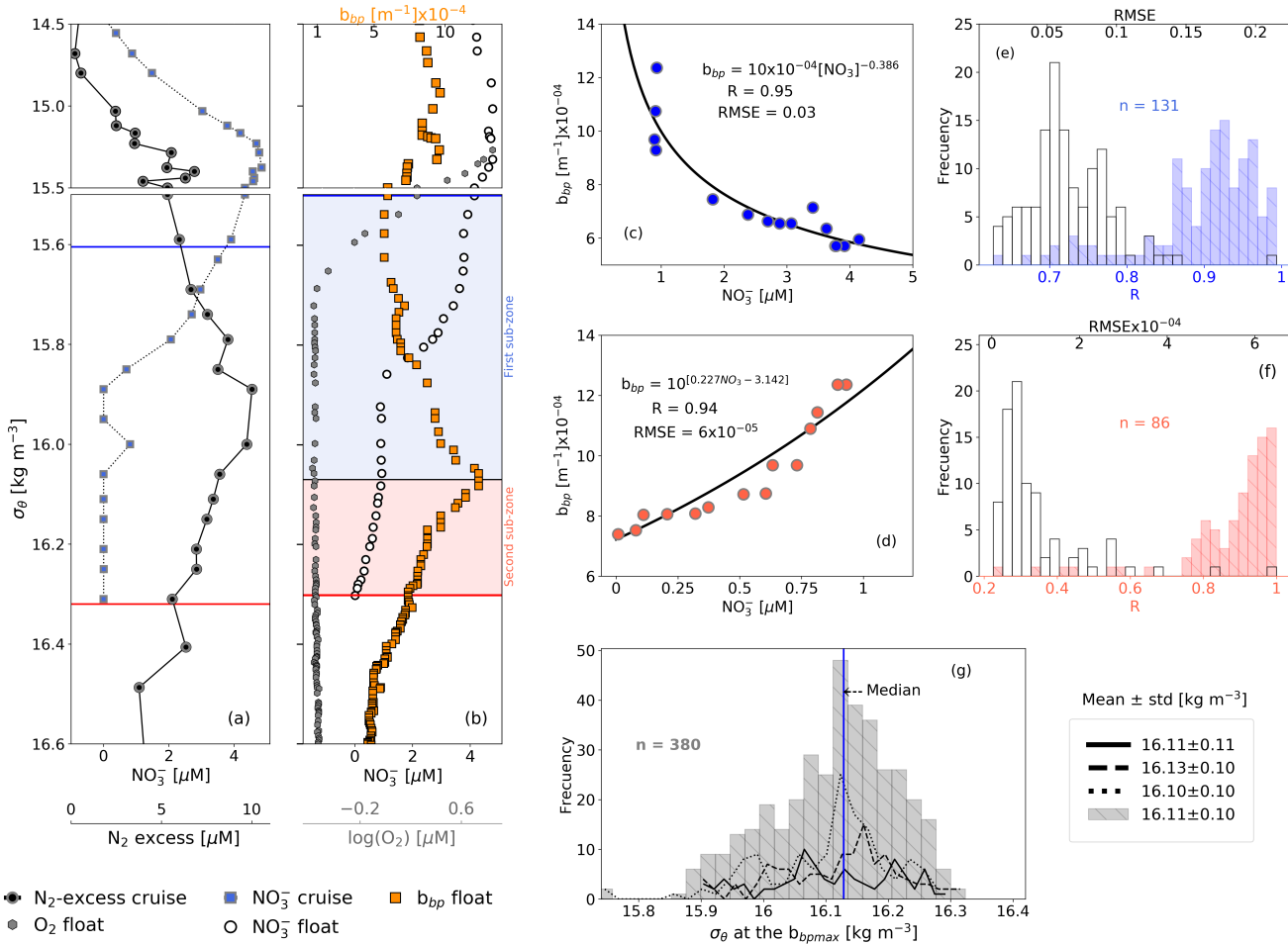
204 We propose that the removal rate of NO_3^- is a key driver of the vertical distribution of small particles and N_2 excess within the
205 $OP_{D,A}$. This is because the vertical profiles of small particles and of N_2 excess are qualitatively similar, and both profiles are
206 clearly related to the rate at which NO_3^- is removed from the $OP_{D,A}$ (Figures 3-4). For instance, maxima of N_2 excess and b_{bp}
207 coincide around the isopycnal $16.11 \pm 0.11 \text{ kg m}^{-3}$ (Figure 3; Konovalov et al., 2005; Fuchsman et al., 2008, 2019). At this
208 isopycnal, the mean concentration of NO_3^- is $1.19 \pm 0.53 \mu\text{M}$. We thus propose that this NO_3^- threshold value splits the $OP_{D,A}$
209 in two sub-zones with distinctive biogeochemical conditions (e.g. nitrogenous and manganous zones; Canfield and Thamdrup,

210 2009). Ultimately, these two different sets of conditions drive the rates at which NO_3^- and small particles are removed and
211 formed within the OP_{D-A} , respectively (Figure 3, and explanation below).

212 The first sub-zone is thus located between the top of the OP_{D-A} ($\sigma_0 = 15.79 \text{ kg m}^{-3}$) and around the isopycnal 16.11 kg m^{-3} .
213 Here, removal rates of NO_3^- ($-0.16 \pm 0.10 \mu\text{M m}^{-1}$, Figure 4) are likely to be boosted by: (1) high content of organic matter
214 (dissolved organic carbon = $122 \pm 9 \mu\text{M}$, Margolin et al., 2016) and NO_3^- ($\geq 1.19 \pm 0.53 \mu\text{M}$), and (2) O_2 levels staying between
215 a range that maintain the yielding of N_2 ($0.24 \pm 0.04 \mu\text{M} \geq \text{O}_2 \leq 2.8 \pm 0.14 \mu\text{M}$, $n = 100$, the means of the minima and maxima
216 of O_2 , respectively, in the first sub-zone) and promote the formation of MnO_2 (e.g. maximum of Mn(II) oxidation is at O_2 levels
217 $\sim 0.2 \mu\text{M}$; Clement et al., 2009). Consequently, the formation of biogenic and inorganic small particles (and related N_2 excess)
218 increases from the top of the OP_{D-A} to around the isopycnal 16.11 kg m^{-3} (Figure 3). This hypothesis is: (1) in part confirmed
219 by significant and negative power-law correlations between the suspended small-particle content and NO_3^- in this sub-zone
220 (Figure 3), and (2) in agreement with the progressive accumulation of MnO_2 from around isopycnal 15.8 kg m^{-3} to the isopycnal
221 16.10 kg m^{-3} (e.g. Konovalov et al., 2006).

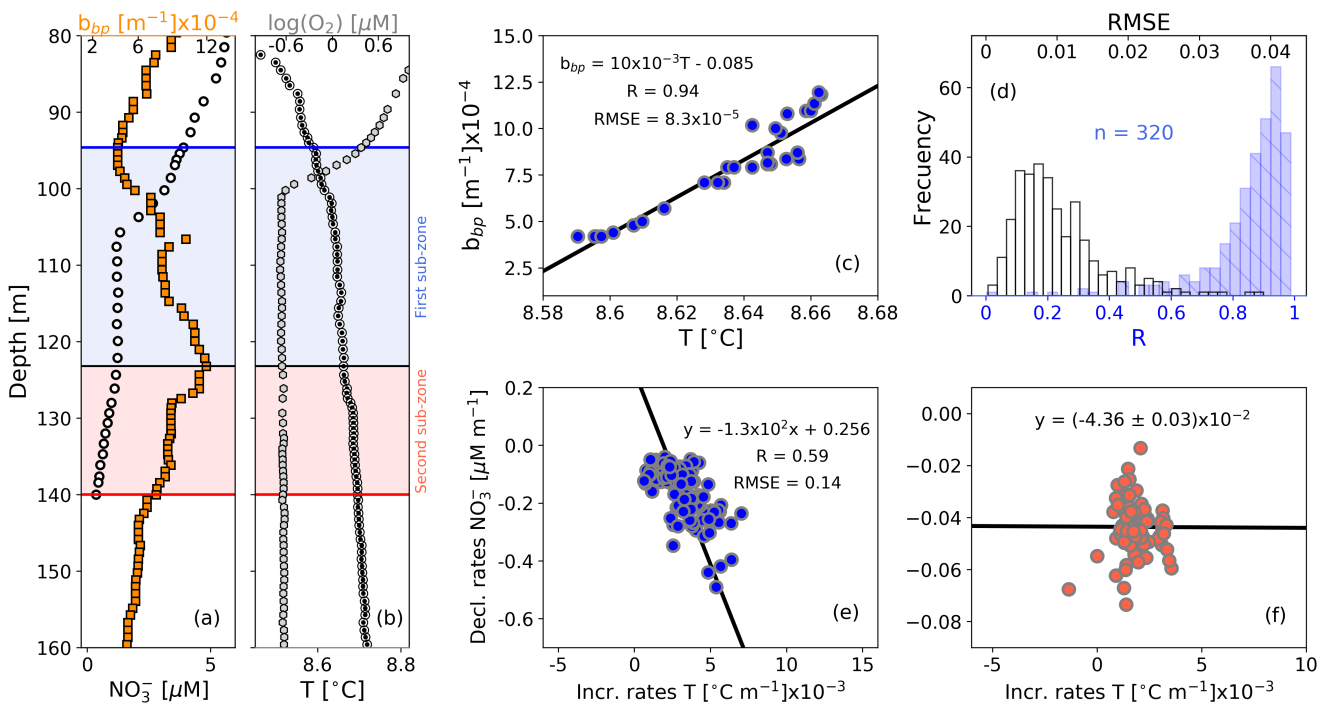
222 The second sub-zone is located between isopycnal 16.11 kg m^{-3} and the bottom of the OP_{D-A} ($\sigma_0 = 16.30 \text{ kg m}^{-3}$, Figure 3).
223 Here, NO_3^- is low ($\leq 1.19 \pm 0.53 \mu\text{M}$) and O_2 is relatively constant ($0.23 \pm 0.02 \mu\text{M}$, $n = 2284$, mean of O_2 calculated in the
224 second sub-zone for all profiles), or lower than the minimum of O_2 recorded by this sensor ($0.22 \pm 0.02 \mu\text{M}$, $n = 89$). These
225 constant (or lower) levels of O_2 roughly correspond to those at which anammox and heterotrophic denitrification are inhibited
226 by $\sim 50\%$ ($0.21 \mu\text{M}$, and $0.81 \mu\text{M}$, respectively; Dalsgaard et al., 2014). In addition, low levels of NO_3^- necessarily promotes
227 the microbial use of Mn(IV) as an electron acceptor, ultimately dissolving the particles of MnO_2 into Mn(II) (e.g. manganous
228 zone; Konovalov et al., 2006; Yakushev et al., 2007; Canfield and Thamdrup, 2009). As a result, this sub-zone exhibits a
229 decline in removal rates of NO_3^- ($-0.04 \pm 0.01 \mu\text{M m}^{-1}$, Figure 4) along with inhibited formation of biogenic small particles and
230 dissolution of MnO_2 . Ultimately, both the content of small particles and related N_2 excess decrease from around isopycnal
231 16.11 kg m^{-3} to the bottom of the OP_{D-A} (Figure 3). These results are in agreement with: (1) significant and positive exponential
232 correlations computed between the small-particle content inferred from b_{bp} and NO_3^- within this sub-zone (Figure 3), and (2)
233 the overlap of nitrogenous and manganous zones in this sub-zone because the content of MnO_2 particles and dissolved Mn(II)
234 concurrently declines and increases just beneath the isopycnal 16.11 kg m^{-3} , respectively (e.g. Murray et al., 1995; Konovalov
235 et al., 2003, 2005, 2006; Yakushev et al., 2007; Canfield and Thamdrup, 2009).

236 Strong-positive linear correlations are also recorded between b_{bp} and T in the first sub-zone of the OP_{D-A} (Figure 4). This is
237 likely to indicate that the formation of small particles is sensitive to very tiny increments in T ($0.003 \pm 0.001 \text{ }^\circ\text{C m}^{-1}$, $n = 133$).
238 We thus infer a tendency for the decline rates of NO_3^- and related production of N_2 to increase with T . This hypothesis is at
239 least partially supported by the significant correlation between NO_3^- decline rates and T increase rates in this sub-zone (Figure
240 4). Within the second sub-zone, T continues increasing while b_{bp} decreases, likely due to inhibition of the formation of small
241 particles for the reasons described above (Figure 4). These observations suggest that the production of small particles is likely
242 to have first- and second-order covariations, with NO_3^- and T , respectively — a likelihood backed up by a lack of correlation
243 between NO_3^- decline rates and T increase rates in this sub-zone (Figure 4). Finally, more information is needed to investigate
244 the physical and/or biogeochemical processes driving the correlation between the increase rates of T , and declines rates of
245 NO_3^- in the first sub-zone. This is however out of the scope of our study.



246

247 **Figure 3: (a) Cruise profiles of NO_3^- , and N_2 excess, collected in March 2005 (Fuchsman et al., 2019). (b) Float profiles**
248 **of NO_3^- , b_{bp} , and $\log(\text{O}_2)$ measured on 6th April 2016. Profiles in (a) and (b) were conducted at the northwest of the basin**
249 **(see Figure 1). The top and bottom of the OP_{D-A} are described in (a) and (b) as horizontal blue and red lines, respectively.**
250 **The b_{bp} maximum is the horizontal black line in (b). The first and second sub-zone of the OP_{D-A} are respectively**
251 **highlighted in (b) as blue and red squares. NO_3^- vs b_{bp} in (c) the first, and (d) the second sub-zone, of the float profile in**
252 **(b). The number of data points visualized in (c) is lower than in (b) for the first sub-zone because b_{bp} and NO_3^- are not**
253 **always recorded at the same depths. (e) Frequency distributions of correlation coefficients (R, blue bars), and root**
254 **mean square errors (RMSE, white bars) for NO_3^- vs b_{bp} in the first sub-zone. (f) Same as (e) but for the second sub-zone.**
255 **(g) Frequency distributions of the isopycnals at which b_{bp} maxima are found within the OP_{D-A} . Dotted, dashed, and solid**
256 **black lines in (g) are data collected by floats 7900591, 6901866, and 6900807, respectively. Gray bars include all data.**



257
258 **Figure 4: Float profiles of (a) NO_3^- , and b_{bp} , and (b) T and $\log(\text{O}_2)$ collected on 10th September 2017. Horizontal blue**

259 and red lines in (a) and (b) are the top and bottom of the OP_{D-A} . The b_{bp} maximum is indicated in (a) and (b) as horizontal

260 black lines. The first and second sub-zones of the OP_{D-A} are respectively highlighted in (a) and (b) as blue and red

261 squares. (c) b_{bp} vs T for the first sub-zone of the profile in (b). (d) Frequency distributions of correlation coefficients (R,

262 blue bars), and root mean square errors (RMSE, white bars), for b_{bp} vs T in the first sub-zone, including data collected

263 by the three floats. Decrease rates of NO_3^- vs increase rates of T in (e) the first and (f) the second sub-zone.

264 To summarize, BGC-Argo float data combined with a proxy of N_2 production suggest that in regions without the Bosphorus
265 plume influence, the b_{bp} -layer systematically tracks and delineates the *effective* N_2 -yielding section independently of: (1) the
266 biogeochemical mechanisms driving N_2 yielding, and (2) the contribution that MnO_2 and other microorganisms can be
267 expected to make to the formation of the b_{bp} -layer (e.g. Lam et al., 2007; Fuchsman et al., 2011; 2012a; Kirkpatrick et al.,
268 2018). It is thus finally inferred that this b_{bp} -layer is *at least partially* composed of the predominant anaerobic microbial
269 communities involved in the production of N_2 , such as *nitrate-reducing SAR11*, and *anammox*, *denitrifying*, and *sulphur-*
270 *oxidizing* bacteria. These results also suggest that N_2 production rates can be highly variable in the Black Sea because the
271 characteristics of the b_{bp} -layer show large spatial-temporal variations driven by changes in NO_3^- and O_2 (Figures 2 and 4).
272 Finally, we propose that b_{bp} and O_2 can be exploited as a combined proxy for defining the N_2 -producing section of the oxygen-
273 poor Black Sea. We consider that this combined proxy can delineate the top and base of this section, by applying an O_2
274 threshold of $3.0 \mu\text{M}$, and the bottom isopycnal of the b_{bp} -layer, respectively. This section should thus be linked to free-living
275 bacteria ($0.2-2 \mu\text{m}$), and those associated with small suspended particles ($> 2-20 \mu\text{m}$), as well as to small inorganic particles
276 ($0.2-20 \mu\text{m}$).

277 4.4 New perspectives for studying N_2 losses in ODZs

278 The conclusions and inferences of this study, especially those related to the origin and drivers of the b_{bp} -layer, primarily apply
279 to the Black Sea. However, these findings may also have a wider application. In particular, the shallower water masses of
280 oxygen-deficient zones (ODZs) are similarly characterized by the formation of a layer of suspended small particles that can

281 be optically detected by b_{bp} and the attenuation coefficients of particles (Spinrad et al., 1989; Naqvi et al., 1993; Whitmire et
282 al., 2009). This layer is mainly linked to N₂-yielding microbial communities because: (1) its location coincides with the maxima
283 of N₂ excess, microbial metabolic activity, and nitrite (NO₂⁻, the intermediate product of denitrification-anammox that is mainly
284 accumulated in the N₂-yielding section, Spinrad et al., 1989; Naqvi et al., 1991, 1993; Devon et al., 2006; Chang et al., 2010,
285 2012; Ulloa et al., 2012; Wojtasiewicz et al., 2018), and (2) MnO₂ is not accumulated as in the Black Sea (Martin and Knauer,
286 1984; Johnson et al., 1996; Lewis and Luther, 2000). Therefore, our findings suggest that highly resolved vertical profiles of
287 b_{bp} and O₂ can potentially be used as a combined proxy to define the *effective* N₂-production section of ODZs. Such definition
288 can be key to better-constrained global estimates of N₂ loss rates because it can allow us to: (1) accurately predict the oxygen-
289 poor water volume where around 90% of N₂ is produced in the ODZ core (Babin et al., 2014), and (2) evaluate how the location
290 and thickness of the N₂-yielding section vary due to changes in the biogeochemical factors that modulate anammox and
291 heterotrophy denitrification.

292 Global estimates of N₂ losses differ by 2-3 fold between studies (e.g. 50-150 Tg N yr⁻¹, Codispoti et al., 2001; Bianchi et al.,
293 2012, 2018; DeVries et al., 2012; Wang et al., 2019). These discrepancies are caused in part by inaccurate estimations of the
294 oxygen-poor volume of the N₂-production section. Other sources of uncertainties arise from the methods applied to estimate
295 the amount of POC that fuels N₂ production. For instance, POC fluxes and their subsequent attenuation rates are not well
296 resolved because they are computed respectively from satellite-based primary-production algorithms and generic power-law
297 functions (Bianchi et al., 2012, 2018; DeVries et al., 2012). POC-flux estimates based on these algorithms visibly exclude: (1)
298 POC supplied by zooplankton migration (Kiko et al., 2017; Tutasi and Escribano, 2020), (2) substantial events of POC export
299 decoupled from primary production (Karl et al., 2012), and (3) the role of small particles derived from the physical and
300 biological fragmentation of larger ones (Karl et al., 1988; Briggs et al., 2020), which are more efficiently remineralized by
301 bacteria in ODZs (Cavan et al., 2017). In addition, these estimates do not take into consideration the inhibition effect that O₂
302 intrusions may have on N₂-yield rates (Whitmire et al., 2009; Ulloa et al., 2012; Dalsgaard et al., 2014; Peters et al., 2016;
303 Margolskee et al., 2019).

304 Overall, mechanistic predictions of N₂ losses misrepresent the strong dynamics of the biogeochemical and physical processes
305 that regulate them. Consequently, it is still debated whether the oceanic nitrogen cycle is in balance or not (Codispoti, 2007;
306 Gruber and Galloway, 2008; DeVries et al., 2012; Jayakumar et al., 2017; Bianchi et al., 2018; Wang et al., 2019). The
307 subsiding uncertainty points to a compelling need for alternative methods that allow accurate refinement of oceanic estimations
308 of N₂ losses.

309 Our study supports the proposition that robotic observations of b_{bp} and O₂ can be used to better delineate the N₂-yielding section
310 at the appropriate spatial (e.g. vertical and regional) and temporal (e.g. event, seasonal, interannual) resolutions. In addition,
311 POC fluxes and N₂ can be simultaneously quantified using the same float technology (BGC-Argo, Bishop et al., 2009;
312 Dall'Olmo and Mork, 2014; Reed et al., 2018; Boyd et al., 2019; Estapa et al., 2019; Rasse and Dall'Olmo, 2019). These
313 robotic measurements can contribute to refining global estimates of N₂ losses by better constraining both the oxygen-poor
314 section where N₂ is produced, and POC fluxes that fuel its loss. Ultimately, O₂ intrusions into the N₂-yielding section can
315 potentially be quantified by BGC-Argo floats to assess their regulatory effect on N₂ losses.

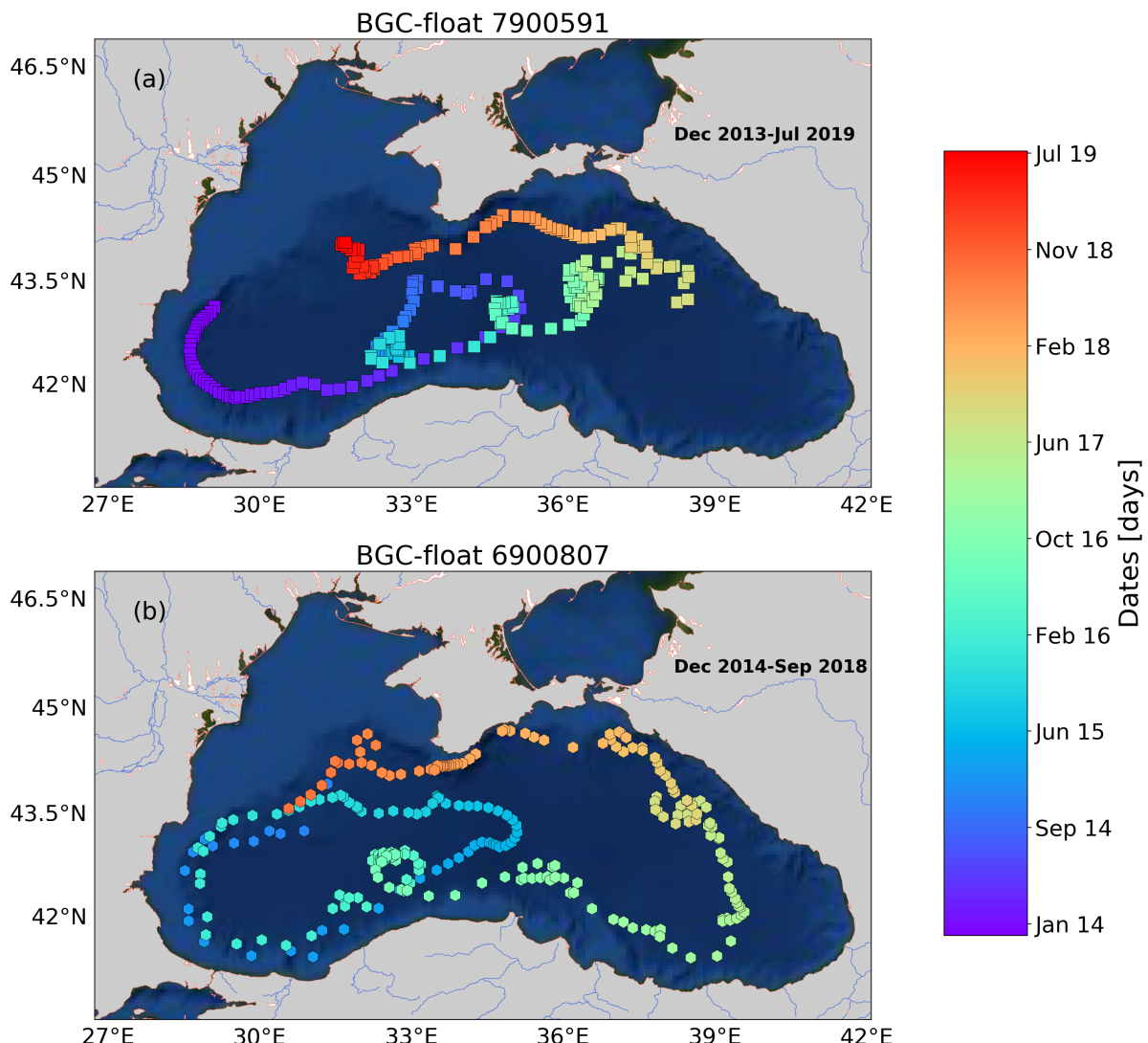
316 **Conclusions**

317 Our results along with those from previous studies suggest that the b_{bp} -layer of the oxygen-poor Black Sea is at least partially
318 composed of nitrate-reducing SAR11, and anammox, denitrifying, and sulphur-oxidizing bacteria. The location and thickness
319 of this layer show strong spatial-temporal variability, mainly driven by the ventilation of oxygen-rich subsurface waters, and

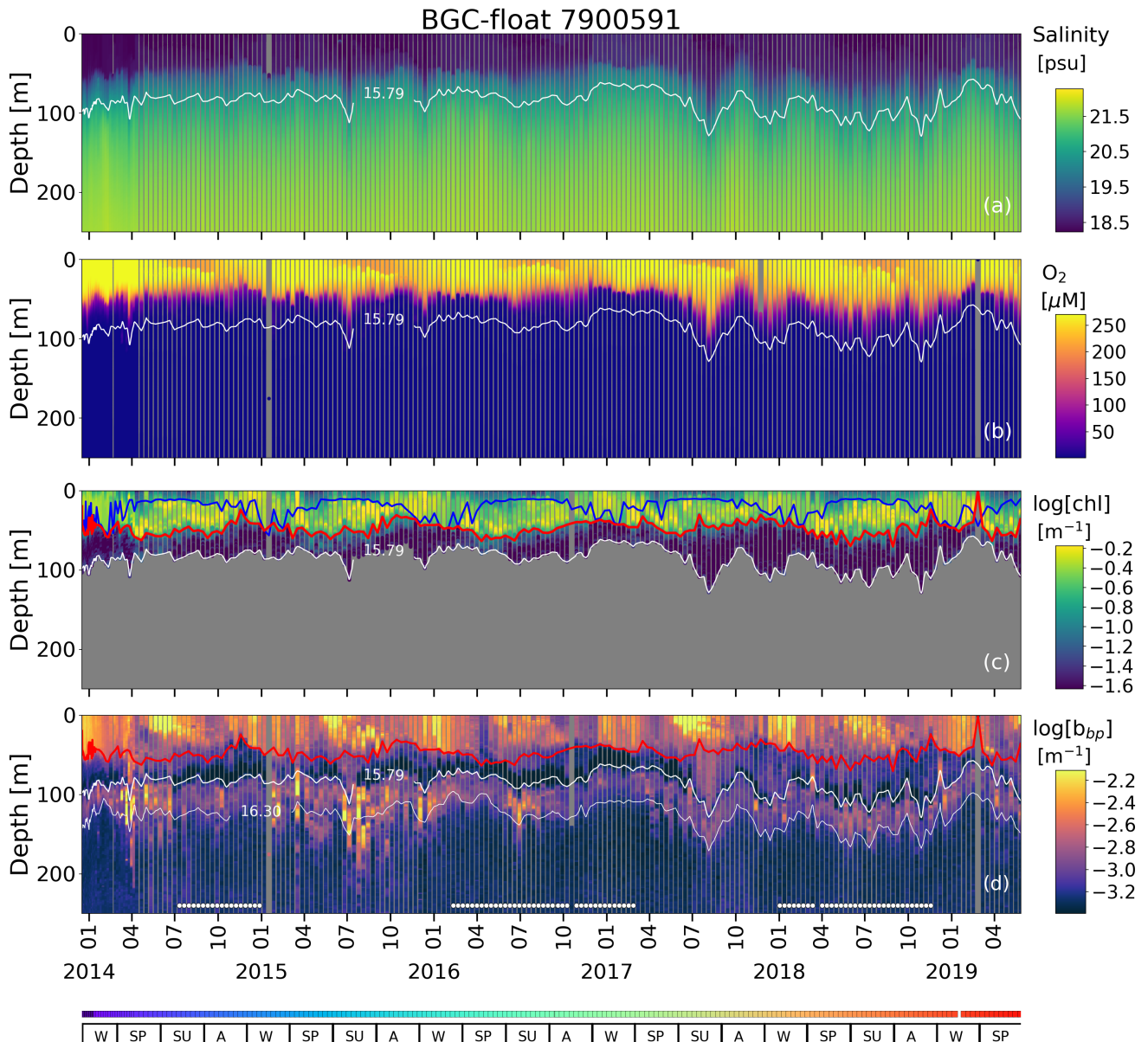
320 nitrate available to generate N_2 , respectively. Such variations in the characteristics of the b_{bp} -layer highlight that N_2 -production
 321 rates can be highly variable in the Black Sea. We therefore propose that high resolution measurements of O_2 and b_{bp} can
 322 potentially be exploited as a combined proxy to delineate the *effective* N_2 -yielding section of ODZs. This proposition is in part
 323 supported by evidence that the b_{bp} -layer and a majority of N_2 -yielding microbial communities are both confined in the
 324 shallower oxygen-poor water masses of ODZs. We however recommend investigation into the key biogeochemical drivers of
 325 the b_{bp} -layer for each ODZ. This information will be critical for validating the applicability of the b_{bp} -layer in assessing spatial-
 326 temporal changes in N_2 production.

327 Finally, it is evident that BGC-Argo float observations can acquire essential proxies of N_2 production and associated drivers
 328 at appropriate spatial and temporal resolutions. The development of observation-modeling synergies therefore holds the
 329 potential to deliver an unprecedented view of N_2 -yielding drivers if robotic observations become an integrated part of model
 330 validation. Ultimately, this approach could prove essential for reducing present uncertainties in the oceanic N_2 budget.

331 **Appendix A: Supplementary Figures**

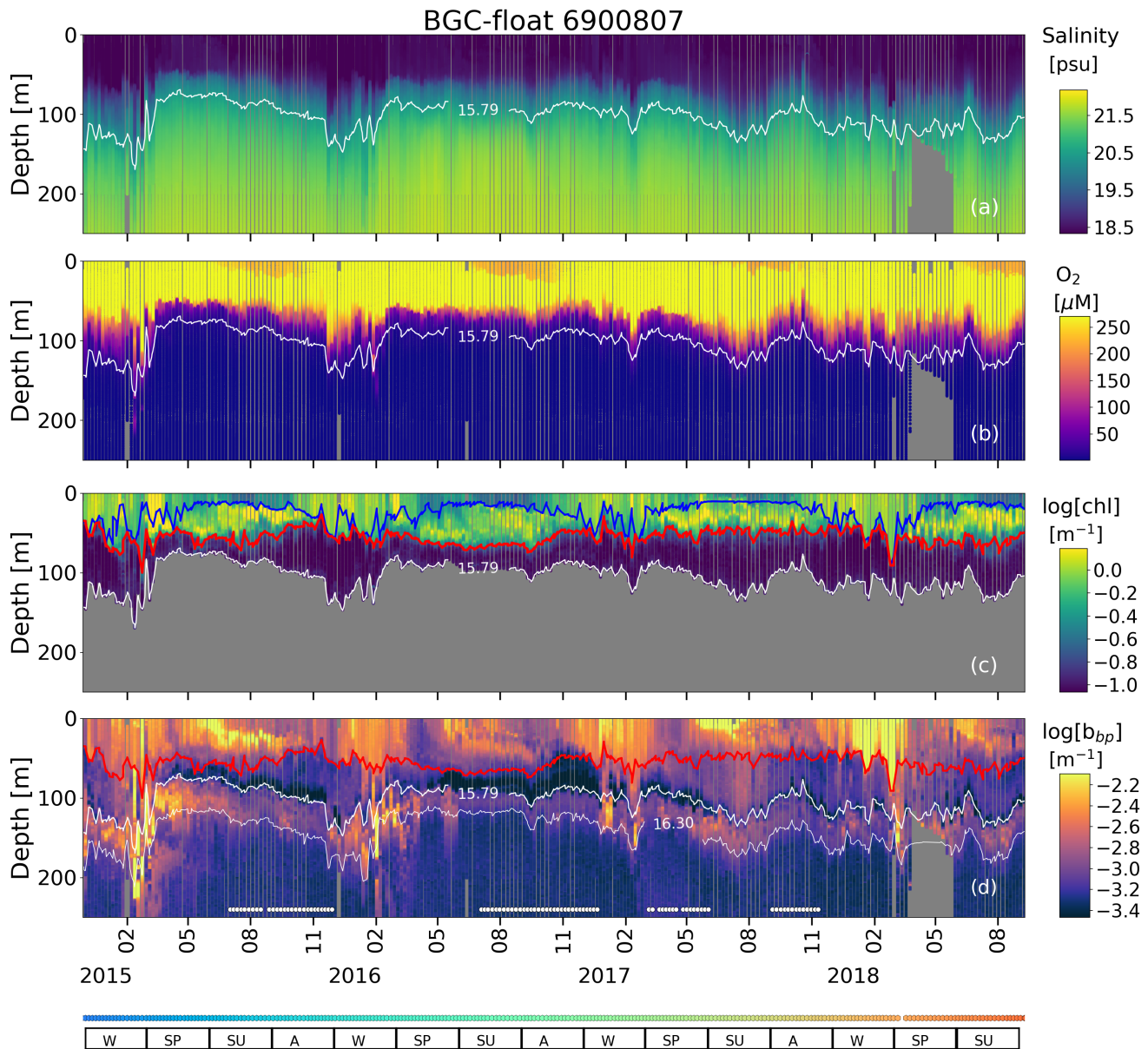


332
 333 **Figure A1: Sampling locations of floats (a) 7900591 and (b) 6900807 between December 2013 and July 2019. Colored**
 334 **squares and hexagons indicate the date (colorbar) for a given profile of floats 6900807 and 7900591, respectively.**



335

336 Figure A2: Time series of (a) S, (b) O₂, (c) log(chl), and (d) log(b_{bp}) for float 7900591. The blue line in (c) indicates the
 337 mixed layer depth. The red lines in (c) and (d) show the base of the productive region. The isopycnals 15.79 kg m⁻³ and
 338 16.30 kg m⁻³ describe the top and bottom of the oxygen-poor zone (*OP_{D-A}*), respectively. SU, A, W, and SP stand for
 339 summer, autumn, winter, and spring, respectively. The colored horizontal line at the bottom indicates the sampling site
 340 for a given date (Figure S1). The horizontal white lines in (d) are the profiles used to: (1) delimit the *OP_{D-A}*, and (2) find
 341 the isopycnals at which b_{bp} is maximum in the *OP_{D-A}*. chl is set to zero in the *OP_{D-A}* due to fluorescence contamination
 342 (Stanev et al., 2017).



343

344 **Figure A3: Same as Figure A2 but for float 6900807**

345 *Data availability.* Data from Biogeochemical-Argo floats used in this study are freely available at <ftp://ifremer.fr/ifremer/argo>.
346 These data were collected and made freely available by the International Argo Program and the national programs that
347 contribute to it (<http://www.argo.ucsd.edu>; the Argo Program is part of the Global Ocean Observing System). Data on N₂:Ar
348 ratios are freely available at <https://agupubs.onlinelibrary.wiley.com/doi/abs/10.1029/2018GB006032>.

349 *Author contributions.* R.R. conceptualized the study, wrote the original draft, and generated all figures. H.C. contributed to
350 tuning the study's conceptualization and figures design. A.P. processed all BGC-Argo float data. R.R. and H.C. reviewed and
351 edited the final manuscript. We finally thank Dr. Clara A. Fuchsman and the anonymous reviewer for their accurate and
352 constructive feedback, which allowed us to significantly improve the original version of the manuscript.

353 *Acknowledgments.* This study was conducted in the framework of the *Noceanic* project. This project is funded by the European
354 Union’s Horizon 2020 research and innovation program under the Marie Skłodowska-Curie Individual Fellowship awarded to
355 Rafael Rasse (grant agreement 839062). This study is a contribution to the remOcean project (European Research Council,

356 grant agreement 246777, Hervé Claustre). Final writing was funded by a European Research Council Advanced grant
357 (REFINE, grant agreement no. 834177).

358 *Competing interests.* The authors declare that they have no conflicts of interest.

359 **References**

360 Alldredge, A. L., and Cohen, Y.: Can microscale chemical patches persist in the sea? Microelectrode study of marine snow,
361 fecal pellets, *Science*, 235(4789), 689-691, DOI: 10.1126/science.235.4789.689, 1987

362 Altabet, M. A., Ryabenko, E., Stramma, L., Wallace, D. W., Frank, M., Grasse, P., and Lavik, G.: An eddy-stimulated hotspot
363 for fixed nitrogen-loss from the Peru oxygen minimum zone, *Biogeosciences*, 9, 4897-4908, <https://doi.org/10.5194/bg-9-4897-2012>, 2012

365 Babbin, A. R., Keil, R. G., Devol, A. H., and Ward, B. B.: Organic matter stoichiometry, flux, and oxygen control nitrogen
366 loss in the ocean, *Science*, 344(6182), 406-408, DOI: 10.1126/science.1248364, 2014.

367 Bianchi, D., Dunne, J. P., Sarmiento, J. L., and Galbraith, E. D.: Data-based estimates of suboxia, denitrification, and N₂O
368 production in the ocean and their sensitivities to dissolved O₂, *Global Biogeochem. Cy.*, 26(2), 2012.

369 Bianchi, D., Weber, T. S., Kiko, R., and Deutsch, C.: Global niche of marine anaerobic metabolisms expanded by particle
370 microenvironments, *Nat. Geosci.*, 11(4), 263-268, <https://doi.org/10.1038/s41561-018-0081-0>, 2018.

371 Bishop, J. K., and Wood, T. J.: Year-round observations of carbon biomass and flux variability in the Southern Ocean, *Global*
372 *Biogeochem. Cy.*, 23(2), <https://doi.org/10.1029/2008GB003206>, 2009.

373 Bittig, H. C., and Körtzinger, A. : Tackling oxygen optode drift: Near-surface and in-air oxygen optode measurements on a
374 float provide an accurate in situ reference, *J. Atmos. Ocean. Technol.*, 32(8), 1536-1543, <https://doi.org/10.1175/JTECH-D-14-00162.1>, 2015.

376 Boyd, P. W., Claustre, H., Levy, M., Siegel, D. A., and Weber, T.: Multi-faceted particle pumps drive carbon sequestration in
377 the ocean, *Nature*, 568(7752), 327-335, <https://doi.org/10.1038/s41586-019-1098-2>, 2019.

378 Briggs, N., Perry, M. J., Cetinić, I., Lee, C., D'Asaro, E., Gray, A. M., and Rehm, E.: High-resolution observations of aggregate
379 flux during a sub-polar North Atlantic spring bloom, *Deep-Sea Res. Pt. I.*, 58(10), 1031–1039,
380 <https://doi.org/10.1016/j.dsr.2011.07.007>, 2011.

381 Briggs, N., Dall'Olmo, G., and Claustre, H.: Major role of particle fragmentation in regulating biological sequestration of CO₂
382 by the oceans, *Science*, 367(6479), 791-793, DOI: 10.1126/science.aay1790, 2020.

383 Bristow, L.A., Dalsgaard, T., Tiano, L., Mills, D.B., Bertagnolli, A.D., Wright, J.J., Hallam, S.J., Ulloa, O., Canfield, D.E.,
384 Revsbech, N.P. and Thamdrup, B.: Ammonium and nitrite oxidation at nanomolar oxygen concentrations in oxygen minimum
385 zone waters, *Proc. Natl. Acad. Sci. U. S. A.*, 113(38), 10601-10606, <https://doi.org/10.1073/pnas.1600359113>, 2016.

386 Bristow, L.A., Callbeck, C.M., Larsen, M., Altabet, M.A., Dekaezemacker, J., Forth, M., Gauns, M., Glud, R.N., Kuypers,
387 M.M., Lavik, G. and Milucka, J.: N₂ production rates limited by nitrite availability in the Bay of Bengal oxygen minimum
388 zone, *Nat. Geosci.*, 10(1), 24-29, <https://doi.org/10.1038/ngeo2847>, 2017.

389 Cavan, E. L., Trimmer, M., Shelley, F., & Sanders, R.: Remineralization of particulate organic carbon in an ocean oxygen
390 minimum zone, *Nat. Commun.*, 8(1), 1-9. <https://doi.org/10.1038/ncomms14847>, 2017.

391 Chang, B. X., Devol, A. H., and Emerson, S. R.: Denitrification and the nitrogen gas excess in the eastern tropical South
392 Pacific oxygen deficient zone, *Deep-Sea Res. Pt. I.*, 57(9), 1092-1101, <https://doi.org/10.1016/j.dsr.2010.05.009>, 2010.

393 Chang, B. X., Devol, A. H., and Emerson, S. R.: Fixed nitrogen loss from the eastern tropical North Pacific and Arabian Sea
394 oxygen deficient zones determined from measurements of N₂:Ar, *Global Biogeochem. Cy.*, 26(3),
395 <https://doi.org/10.1029/2011GB004207>, 2012.

396 Callbeck, C.M., Lavik, G., Ferdelman, T.G., Fuchs, B., Gruber-Vodicka, H.R., Hach, P.F., Littmann, S., Schoffelen, N.J.,
397 Kalvelage, T., Thomsen, S. and Schunck, H.: Oxygen minimum zone cryptic sulfur cycling sustained by offshore transport of
398 key sulfur oxidizing bacteria, *Nat. Commun.*, 9(1), 1-11, <https://doi.org/10.1038/s41467-018-04041-x>, 2018.

399 Canfield, D. E., and Thamdrup, B.: Towards a consistent classification scheme for geochemical environments, or, why we
400 wish the term ‘suboxic’ would go away, *Geobiology*, 7(4), 385-392. <https://doi.org/10.1111/j.1472-4669.2009.00214.x>, 2009.

401 Canfield, D.E., Stewart, F.J., Thamdrup, B., De Brabandere, L., Dalsgaard, T., Delong, E.F., Revsbech, N.P. and Ulloa, O.: A
402 cryptic sulfur cycle in oxygen-minimum-zone waters off the Chilean coast, *Science*, 330(6009), 1375-1378, DOI:
403 10.1126/science.1196889, 2010.

404 Clement, B. G., Luther, G. W., and Tebo, B. M.: Rapid, oxygen-dependent microbial Mn (II) oxidation kinetics at sub-
405 micromolar oxygen concentrations in the Black Sea suboxic zone, *Geochim. Cosmochim. Acta*, 73(7), 1878-1889.
406 <https://doi.org/10.1016/j.gca.2008.12.023>, 2009.

407 Codispoti, L. A.: An oceanic fixed nitrogen sink exceeding 400 Tg N a⁻¹ vs the concept of homeostasis in the fixed-nitrogen
408 inventory, *Biogeosciences*, 4, 233–253, <https://doi.org/10.5194/bg-4-233-2007>, 2007.

409 Codispoti, L. A., Brandes, J. A., Christensen, J. P., Devol, A. H., Naqvi, S. W. A., Paerl, H. W., and Yoshinari, T.: The oceanic
410 fixed nitrogen and nitrous oxide budgets: Moving targets as we enter the anthropocene?, *Sci. Mar.*, 65(S2), 85-105, 2007.

411 Çoban-Yıldız, Y., Altabet, M. A., Yılmaz, A., and Tuğrul, S.: Carbon and nitrogen isotopic ratios of suspended particulate
412 organic matter (SPOM) in the Black Sea water column, *Deep Sea Res. Part II Top. Stud. Oceanogr.*, 53(17-19), 1875-1892,
413 <https://doi.org/10.1016/j.dsr2.2006.03.021>, 2006.

414 Dall'Olmo, G., and Mork, K. A.: Carbon export by small particles in the Norwegian Sea, *Geophys. Res. Lett.*, 41, 2921–2927,
415 <https://doi.org/10.1002/2014GL059244>, 2014.

416 Dalsgaard, T., Stewart, F.J., Thamdrup, B., De Brabandere, L., Revsbech, N.P., Ulloa, O., Canfield, D.E. and DeLong, E.F.:
417 Oxygen at nanomolar levels reversibly suppresses process rates and gene expression in anammox and denitrification in the
418 oxygen minimum zone off northern Chile, *MBio.*, 5(6), e01966-14, 10.1128/mBio.01966-14, 2014.

419 Dalsgaard, T., Thamdrup, B., Farías, L., and Revsbech, N. P.: Anammox and denitrification in the oxygen minimum zone of
420 the eastern South Pacific, *Limnol. Oceanogr.*, 57(5), 1331-1346, <https://doi.org/10.4319/lo.2012.57.5.1331>, 2012.

421 de Boyer Montégut, C., Madec, G., Fischer, A. S., Lazar, A., and Iudicone, D.: Mixed layer depth over the global ocean: An
422 examination of profile data and a profile-based climatology, *J. Geophys. Res. Oceans*, 109(C12),
423 <https://doi.org/10.1029/2004JC002378>, 2004.

424 Dellwig, O., Leipe, T., Ma, C., Glockzin, M., Pollehne, F., Schnetger, B., Yakushev, E. V., and Bo, M. E.: A new particulate
425 Mn – Fe – P-shuttle at the redoxcline of anoxic basins, *Geochim. Cosmochim. Ac.*, 74, 7100–7115.
426 <https://doi.org/10.1016/j.gca.2010.09.017>, 2010.

427 DeVries, T., Deutsch, C., Primeau, F., Chang, B., and Devol, A.: Global rates of water-column denitrification derived from
428 nitrogen gas measurements, *Nat. Geosci.*, 5(8), 547–550, <https://doi.org/10.1038/ngeo1515>, 2012.

429 DeVries, T., Deutsch, C., Rafter, P. A., and Primeau, F.: Marine denitrification rates determined from a global 3-D inverse
430 model, *Biogeosciences*, 10(4), 2481–2496. <https://doi.org/10.5194/bg-10-2481-2013>, 2013

431 Ediger, D., Murray, J. W., and Yilmaz, A.: Phytoplankton biomass, primary production and chemoautotrophic production of
432 the Western Black Sea in April 2003. *J. Mar. Syst.*, 198, 103183, <https://doi.org/10.1016/j.jmarsys.2019.103183>, 2019.

433 Estapa, M. L., Feen, M. L., and Breves, E.: Direct observations of biological carbon export from profiling floats in the
434 subtropical North Atlantic, *Global Biogeochem. Cy.*, 33(3), 282–300, <https://doi.org/10.1029/2018GB006098>, 2019.

435 Fuchsman, C. A., Devol, A. H., Saunders, J. K., McKay, C., and Rocap, G.: Niche partitioning of the N cycling microbial
436 community of an offshore oxygen deficient zone, *Front. Microbiol.*, 8, 2384, <https://doi.org/10.3389/fmicb.2017.02384>, 2017.

437 Fuchsman, C. A., Kirkpatrick, J. B., Brazelton, W. J., Murray, J. W., and Staley, J. T.: Metabolic strategies of free-living and
438 aggregate-associated bacterial communities inferred from biologic and chemical profiles in the Black Sea suboxic zone. *FEMS*
439 *Microbiol. Ecol.*, 78, 586–603, <https://doi.org/10.1111/j.1574-6941.2011.01189.x>, 2011.

440 Fuchsman, C. A., Murray, J. W., and Konovalov, S. K.: Concentration and natural stable isotope profiles of nitrogen species
441 in the Black Sea, *Mar. Chem.*, 111(1–2), 90–105, <https://doi.org/10.1016/j.marchem.2008.04.009>, 2008.

442 Fuchsman, C. A., Murray, J. W., and Staley, J. T.: Stimulation of autotrophic denitrification by intrusions of the Bosphorus
443 Plume into the anoxic Black Sea, *Front. Microbiol.*, 3, 257, <https://doi.org/10.3389/fmicb.2012.00257>, 2012b.

444 Fuchsman, C. A., Paul, B., Staley, J. T., Yakushev, E. V., and Murray, J. W.: Detection of transient denitrification during a
445 high organic matter event in the Black Sea, *Global Biogeochem. Cy.*, 33(2), 143–162, <https://doi.org/10.1029/2018GB006032>,
446 2019.

447 Fuchsman, C. A., Staley, J. T., Oakley, B. B., Kirkpatrick, J. B., and Murray, J. W.: Free-living and aggregate-associated
448 Planctomycetes in the Black Sea, *FEMS Microbiol. Ecol.*, 80(2), 402–416, <https://doi.org/10.1111/j.1574-6941.2012.01306.x>,
449 2012a.

450 Ganesh, S., Bristow, L. A., Larsen, M., Sarode, N., Thamdrup, B., and Stewart, F. J.: Size-fraction partitioning of community
451 gene transcription and nitrogen metabolism in a marine oxygen minimum zone, *ISME J.*, 9(12), 2682,
452 <https://doi.org/10.1038/ismej.2015.44>, 2015.

453 Ganesh, S., Parris, D. J., DeLong, E. F., and Stewart, F. J.: Metagenomic analysis of size-fractionated picoplankton in a marine
454 oxygen minimum zone, *ISME J.*, 8(1), 187, <https://doi.org/10.1038/ismej.2013.144>, 2014.

455 Gaye, B., Nagel, B., Dähnke, K., Rixen, T., and Emeis, K. C.: Evidence of parallel denitrification and nitrite oxidation in the
456 ODZ of the Arabian Sea from paired stable isotopes of nitrate and nitrite, *Global Biogeochem. Cy.*, 27(4), 1059-1071,
457 <https://doi.org/10.1002/2011GB004115>, 2013.

458 Glaubitz, S., Labrenz, M., Jost, G., and Jürgens, K.: Diversity of active chemolithoautotrophic prokaryotes in the sulfidic zone
459 of a Black Sea pelagic redoxcline as determined by rRNA-based stable isotope probing, *FEMS Microbiol. Ecol.*, 74(1), 32-
460 41, <https://doi.org/10.1111/j.1574-6941.2010.00944.x>, 2010.

461 Grote, J., Jost, G., Labrenz, M., Herndl, G. J., and Jürgens, K.: Epsilonproteobacteria represent the major portion of
462 chemoautotrophic bacteria in sulfidic waters of pelagic redoxclines of the Baltic and Black Seas, *Appl. Environ. Microbiol.*,
463 74(24), 7546-7551, DOI: 10.1128/AEM.01186-08, 2008.

464 Gruber, N., and Sarmiento, J. L.: Global patterns of marine nitrogen fixation and denitrification, *Global Biogeochem. Cy.*,
465 11(2), 235-266, <https://doi.org/10.1029/97GB00077>, 1997.

466 Gruber, N., and Galloway, J. N.: An Earth-system perspective of the global nitrogen cycle, *Nature*, 451(7176), 293-296,
467 <https://doi.org/10.1038/nature06592>, 2008.

468 Hamme, R. C., and Emerson, S. R.: The solubility of neon, nitrogen and argon in distilled water and seawater, *Deep-Sea Res.*
469 Pt. I., 51(11), 1517-1528, <https://doi.org/10.1016/j.dsr.2004.06.009>, 2004.

470 Helm, K. P., Bindoff, N. L., and Church, J. A.: Observed decreases in oxygen content of the global ocean, *Geophys. Res. Lett.*,
471 38(23), <https://doi.org/10.1029/2011GL049513>, 2011.

472 Jayakumar, A., Chang, B. X., Widner, B., Bernhardt, P., Mulholland, M. R., and Ward, B. B.: Biological nitrogen fixation in
473 the oxygen-minimum region of the eastern tropical North Pacific ocean, *ISME J.*, 11(10), 2356-2367,
474 <https://doi.org/10.1038/ismej.2017.97>, 2017.

475 Jensen, M. M., Kuypers, M. M., Gaute, L., and Thamdrup, B.: Rates and regulation of anaerobic ammonium oxidation and
476 denitrification in the Black Sea, *Limnol. Oceanogr.*, 53(1), 23-36, <https://doi.org/10.4319/lo.2008.53.1.0023>, 2008.

477 Johnson, K. S.: Manganese redox chemistry revisited. *Science*, 313(5795), 1896-1897, DOI: 10.1126/science.1133496, 2006.

478 Johnson, K. S., Coale, K. H., Berelson, W. M., and Gordon, R. M.: On the formation of the manganese maximum in the oxygen
479 minimum, *Geochim. Cosmochim. Acta.*, 60(8), 1291-1299, [https://doi.org/10.1016/0016-7037\(96\)00005-1](https://doi.org/10.1016/0016-7037(96)00005-1), 1996.

480 Johnson, K. S., Pasqueron de Fommervault, O., Serra, R., D'Ortenzio, F., Schmechtig, C., Claustre, H., and Poteau, A.:
481 Processing Bio-Argo nitrate concentration at the DAC level, doi:10.13155/46121, 2018.

483 Karl, D. M., Church, M. J., Dore, J. E., Letelier, R. M., and Mahaffey, C.: Predictable and efficient carbon sequestration in the
484 North Pacific Ocean supported by symbiotic nitrogen fixation, *Proc. Natl. Acad. Sci. U. S. A.*, 109(6), 1842-1849,
485 <https://doi.org/10.1073/pnas.1120312109>, 2012.

486 Karl, D. M., Knauer, G. A., and Martin, J. H.: Downward flux of particulate organic matter in the ocean: a particle
487 decomposition paradox, *Nature*, 332(6163), 438-441, <https://doi.org/10.1038/332438a0>, 1988.

488 Karstensen, J., Stramma, L., and Visbeck, M.: Oxygen minimum zones in the eastern tropical Atlantic and Pacific oceans,
489 *Prog. Oceanogr.*, 77(4), 331-350, <https://doi.org/10.1016/j.pocean.2007.05.009>, 2008.

490 Keeling, R. F., and Garcia, H. E.: The change in oceanic O₂ inventory associated with recent global warming, *Proc. Natl. Acad.*
491 *Sci. U. S. A.*, 99(12), 7848-7853, <https://doi.org/10.1073/pnas.122154899>, 2002.

492 Kiko, R., Biastoch, A., Brandt, P., Cravatte, S., Hauss, H., Hummels, R., Kriest, I., Marin, F., McDonnell, A.M.P., Oschlies,
493 A. and Picheral, M.: Biological and physical influences on marine snowfall at the equator, *Nat. Geosci.*, 10(11), 852-858,
494 <https://doi.org/10.1038/ngeo3042>, 2017.

495 Kirkpatrick, J. B., Fuchsman, C. A., Yakushev, E., Staley, J. T., and Murray, J. W.: Concurrent activity of anammox and
496 denitrifying bacteria in the Black Sea, *Front. Microbiol.*, 3, 256, <https://doi.org/10.3389/fmicb.2012.00256>, 2012.

497 Kirkpatrick, J. B., Fuchsman, C. A., Yakushev, E. V., Egorov, A. V., Staley, J. T., and Murray, J. W.: Dark N₂ fixation: nifH
498 expression in the redoxcline of the Black Sea, *Aquat. Microb. Ecol.*, 82, 43–58. <https://doi.org/10.3354/ame01882>, 2018.

499 Konovalov, S.K., Luther, G.I.W., Friederich, G.E., Nuzzio, D.B., Tebo, B.M., Murray, J.W., Oguz, T., Glazer, B., Trouwborst,
500 R.E., Clement, B. and Murray, K.J.: Lateral injection of oxygen with the Bosphorus plume—fingers of oxidizing potential in
501 the Black Sea, *Limnol. Oceanogr.*, 48(6), 2369-2376, <https://doi.org/10.4319/lo.2003.48.6.2369>, 2003.

502 Konovalov, S. K., Murray, J. W., and Luther III, g. W.: Black Sea Biogeochemistry, *Oceanography*, 18(2), 24,
503 <https://doi.org/10.5670/oceanog.2005.39>, 2005.

504 Konovalov, S. K., Murray, J. W., Luther, G. W., and Tebo, B. M.: Processes controlling the redox budget for the oxic/anoxic
505 water column of the Black Sea, *Deep-Sea Res. Pt. II.*, 53(17-19), 1817-1841, <https://doi.org/10.1016/j.dsr2.2006.03.013>, 2006.

506 Kuypers, M.M., Sliekers, A.O., Lavik, G., Schmid, M., Jørgensen, B.B., Kuenen, J.G., Damsté, J.S.S., Strous, M. and Jetten,
507 M.S.: Anaerobic ammonium oxidation by anammox bacteria in the Black Sea, *Nature*, 422(6932), 608,
508 <https://doi.org/10.1038/nature01472>, 2003.

509 Lam, P., Jensen, M. M., Lavik, G., McGinnis, D. F., Müller, B., Schubert, C. J., Amann, R., Thamdrup, B., and Kuypers, M.
510 M.: Linking crenarchaeal and bacterial nitrification to anammox in the Black Sea, *Proc. Natl. Acad. Sci. U. S. A.*, 104(17),
511 7104-7109. <https://doi.org/10.1073/pnas.0611081104>, 2007.

512 Lam, P., Lavik, G., Jensen, M.M., van de Vossenberg, J., Schmid, M., Woebken, D., Gutiérrez, D., Amann, R., Jetten, M.S.
513 and Kuypers, M.M.: Revising the nitrogen cycle in the Peruvian oxygen minimum zone, *Proc. Natl. Acad. Sci. U. S. A.*,
514 106(12), 4752-4757, <https://doi.org/10.1073/pnas.0812444106>, 2009.

515 Lewis, B. L., and Luther III, G. W.: Processes controlling the distribution and cycling of manganese in the oxygen minimum
516 zone of the Arabian Sea, *Deep Sea Res. Part II Top. Stud. Oceanogr.*, 47(7-8), 1541-1561, [https://doi.org/10.1016/S0967-0645\(99\)00153-8](https://doi.org/10.1016/S0967-0645(99)00153-8), 2000.

518 Margolin, A. R., Gerringa, L. J., Hansell, D. A., and Rijkenberg, M. J.: Net removal of dissolved organic carbon in the anoxic
519 waters of the Black Sea, *Mar. Chem.*, 183, 13-24, <https://doi.org/10.1016/j.marchem.2016.05.003>, 2016.

520 Margolskee, A., Frenzel, H., Emerson, S., and Deutsch, C. :Ventilation pathways for the North Pacific oxygen deficient zone, 521 Global Biogeochem. Cy., 33(7), 875-890. <https://doi.org/10.1029/2018GB006149>, 2019.

522 Martin, J. H., & Knauer, G. A.: VERTEX: manganese transport through oxygen minima; Earth Planet. Sci., 67(1), 35-47m 523 [https://doi.org/10.1016/0012-821X\(84\)90036-0](https://doi.org/10.1016/0012-821X(84)90036-0), 1984

524 Murray, J. W., Codispoti, L. A., and Friederich, G. E.: Oxidation-reduction environments: The suboxic zone in the Black Sea, 525 In C. P. Huang, C. R. O'Melia, and J. J. Morgan (Eds.), Aquatic chemistry: Interfacial and interspecies processes, ACS 526 Advances in Chemistry Series (Vol. 224, pp. 157–176), Washington DC: American Chemical Society, 1995.

527 Murray, J. W., Fuchsman, C., Kirkpatrick, J., Paul, B., and Konovalov, S. K.: Species and $\delta^{15}\text{N}$ Signatures of nitrogen 528 Transformations in the Suboxic Zone of the Black Sea, Oceanography., 18(2), 36-47, <https://doi.org/10.5670/oceanog.2005.40>, 529 2005.

530 Naqvi, S.W.A.: Geographical extent of denitrification in the Arabian Sea, Oceanol. Acta, 14(3), 281-290, 1991

531 Naqvi, S. W. A., Kumar, M. D., Narvekar, P. V., De Sousa, S. N., George, M. D., and D'silva, C.: An intermediate nepheloid 532 layer associated with high microbial metabolic rates and denitrification in the northwest Indian Ocean, J. Geophys. Res. 533 Oceans, 98(C9), 16469-16479, <https://doi.org/10.1029/93JC00973>, 1993.

534 Organelli, E., Dall'Olmo, G., Brewin, R. J., Tarran, G. A., Boss, E., and Bricaud, A.: The open-ocean missing backscattering 535 is in the structural complexity of particles, Nat. Commun., 9(1), 1–11. <https://doi.org/10.1038/s41467-018-07814-6>, 2018.

536 Oschlies, A., Brandt, P., Stramma, L., and Schmidtko, S.: Drivers and mechanisms of ocean deoxygenation, Nat. Geosci., 537 11(7), 467-473, <https://doi.org/10.1038/s41561-018-0152-2>, 2018.

538 Peters, B. D., Babbin, A. R., Lettmann, K. A., Mordy, C. W., Ulloa, O., Ward, B. B., and Casciotti, K. L.: Vertical modeling 539 of the nitrogen cycle in the eastern tropical South Pacific oxygen deficient zone using high-resolution concentration and isotope 540 measurements, Global Biogeochem. Cy., 30(11), 1661-1681, <https://doi.org/10.1002/2016GB005415>, 2016.

541 Rasse, R., and Dall'Olmo, G.: Do oceanic hypoxic regions act as barriers for sinking particles? A case study in the eastern 542 tropical north Atlantic, Global Biogeochem. Cy., <https://doi.org/10.1029/2019GB006305>, 2019.

543 Reed, A., McNeil, C., D'Asaro, E., Altabet, M., Bourbonnais, A., and Johnson, B.: A gas tension device for the mesopelagic 544 zone, Deep Sea Res. Part I Oceanogr. Res. Pap., 139, 68-78. <https://doi.org/10.1016/j.dsr.2018.07.007>, 2018.

545 Schmechtig, C., Claustre, H., Poteau, A., and D'Ortenzio, F.: Bio-Argo quality control manual for the chlorophyll-a 546 concentration, (pp.1–13), Argo Data Management. <https://doi.org/10.13155/35385>, 2014.

547 Schmechtig, C., Poteau, A., Claustre, H., D'ortenzio, F., Giorgio Dall'Olmo, G., and Boss E.: Processing BGC-Argo particle 548 backscattering at the DAC level, <https://doi.org/10.13155/39459>, 2015.

549 Schmidtko, S., Stramma, L., and Visbeck, M. Decline in global oceanic oxygen content during the past five decades. Nature, 550 542(7641), 335–339, <https://doi.org/10.1038/nature21399>, 2017.

551 Sorokin, Y. I.:The Black Sea: ecology and oceanography. 2002.

552 Spinrad, R. W., Glover, H., Ward, B. B., Codispoti, L. A., and Kullenberg, G.: Suspended particle and bacterial maxima in
553 Peruvian coastal waters during a cold water anomaly, *Deep-Sea Res. Pt. I.*, 36(5), 715-733, 1989.

554 Stanev, E. V., Grayek, S., Claustre, H., Schmechtig, C., and Poteau, A.: Water intrusions and particle signatures in the Black
555 Sea: a Biogeochemical-Argo float investigation, *Ocean Dyn.*, 67(9), 1119-1136, <https://doi.org/10.1007/s10236-017-1077-9>,
556 2017.

557 Stanev, E. V., Poulain, P. M., Grayek, S., Johnson, K. S., Claustre, H., and Murray, J. W.: Understanding the Dynamics of the
558 Oxic-Anoxic Interface in the Black Sea, *Geophys. Res. Lett.*, 45(2), 864-871, <https://doi.org/10.1002/2017GL076206>, 2018.

559 Stramma, L., Johnson, G. C., Sprintall, J., and Mohrholz, V.: Expanding oxygen-minimum zones in the tropical oceans.
560 *Science*, 320(5876), 655-658, <https://doi.org/10.1126/science.1153847>, 2008.

561 Stramski, D., Boss, E., Bogucki, D., and Voss, K. J.: The role of seawater constituents in light backscattering in the ocean.
562 *Prog. Oceanogr.*, 61(1), 27-56, <https://doi.org/10.1016/j.pocean.2004.07.001>, 2004.

563 Stramski, D., Reynolds, R. A., Kahru, M., and Mitchell, B. G.: Estimation of particulate organic carbon in the ocean from
564 satellite remote sensing, *Science*, 285(5425), 239-242, DOI: 10.1126/science.285.5425.239, 1999.

565 Stumm, W., and Morgan, J.J.: *Aquatic Chemistry: An Introduction Emphasizing Chemical Equilibria in Natural Waters*,
566 Wiley-Interscience, New York, 1970.

567 Thierry, V., Bittig, H., and Argo BGC Team.: Argo quality control manual for dissolved oxygen concentration. Version 2.0,
568 23 October 2018. 10.13155/46542, 2018.

569 Tsementzi, D., Wu, J., Deutsch, S., Nath, S., Rodriguez-R, L. M., Burns, A. S., Ranjan, P., Sarode, N., Malmstrom, R.R.,
570 Padilla, C.C., nad Stone, B. K.: SAR11 bacteria linked to ocean anoxia and nitrogen loss, *Nature*, 536(7615), 179-183,
571 <https://doi.org/10.1038/nature19068>, 2016.

572 Tutasi, P., and Escribano, R.: Zooplankton diel vertical migration and downward C into the Oxygen Minimum Zone in the
573 highly productive upwelling region off Northern Chile, *Biogeosciences*, 17, 455-473, <https://doi.org/10.5194/bg-17-455-2020>, 2020.

575 Ulloa, O., Canfield, D. E., DeLong, E. F., Letelier, R. M., and Stewart, F. J.: Microbial oceanography of anoxic oxygen
576 minimum zones, *Proc. Natl. Acad. Sci. U. S. A.*, 109(40), 15996-16003, <https://doi.org/10.1073/pnas.1205009109>, 2012.

577 Wang, W. L., Moore, J. K., Martiny, A. C., and Primeau, F. W.: Convergent estimates of marine nitrogen fixation, *Nature*,
578 566(7743), 205-211, <https://doi.org/10.1038/s41586-019-0911-2>, 2019.

579 Ward, B. B. How nitrogen is lost, *Science*, 341(6144), 352-353, DOI: 10.1126/science.1240314, 2013.

580 Ward, B.B., Devol, A.H., Rich, J.J., Chang, B.X., Bulow, S.E., Naik, H., Pratihary, A. and Jayakumar, A.: Denitrification as
581 the dominant nitrogen loss process in the Arabian Sea, *Nature*, 461(7260), 78-81, <https://doi.org/10.1038/nature08276>, 2009.

582 Ward, B. B., and Kilpatrick, K. A.: Nitrogen transformations in the oxic layer of permanent anoxic basins: the Black Sea and
583 the Cariaco Trench, In *Black Sea Oceanography*, Springer, Dordrecht, 111-124, https://doi.org/10.1007/978-94-011-2608-3_7,
584 1991.

585 Ward, B. B., Tuit, C. B., Jayakumar, A., Rich, J. J., Moffett, J., and Naqvi, S. W. A.: Organic carbon, and not copper, controls
586 denitrification in oxygen minimum zones of the ocean, *Deep-Sea Res. Pt. I.*, 55(12), 1672-1683,
587 <https://doi.org/10.1016/j.dsr.2008.07.005>, 2008.

588 Whitmire, A. L., Letelier, R. M., Villagrán, V., and Ulloa, O.: Autonomous observations of in vivo fluorescence and particle
589 backscattering in an oceanic oxygen minimum zone, *Opt. Express*, 17(24), 21, 992–22,004.
590 <https://doi.org/10.1364/OE.17.021992>, 2009.

591 Wojtasiewicz, B., Trull, T. W., Bhaskar, T. U., Gauns, M., Prakash, S., Ravichandran, M., and Hardman-Mountford, N. J.:
592 Autonomous profiling float observations reveal the dynamics of deep biomass distributions in the denitrifying oxygen
593 minimum zone of the Arabian Sea, *J. Mar. Syst.*, <https://doi.org/10.1016/j.jmarsys.2018.07.002>, 2018.

594 Yakushev, E. V., Pollehn, F., Jost, G., Kuznetsov, I., Schneider, B., and Umlauf, L.: Analysis of the water column oxic/anoxic
595 interface in the Black and Baltic seas with a numerical model, *Mar. Chem.*, 107(3), 388-410,
596 <https://doi.org/10.1016/j.marchem.2007.06.003>, 2007.

597 Yılmaz, A., Çoban-Yıldız, Y., Telli-Karakoç, F., and Bologa, A.: Surface and mid-water sources of organic carbon by
598 photoautotrophic and chemoaautotrophic production in the Black Sea. *Deep Sea Research Part II: Topical Studies in*
599 *Oceanography*, 53(17-19), 1988-2004, *Deep Sea Res. Part II Top. Stud. Oceanogr.*, <https://doi.org/10.1016/j.dsr2.2006.03.015>,
600 2006.